Sensors and Actuators A 234 (2015) 23–33

Contents lists available at ScienceDirect

Sensors and Actuators A: Physical

journal homepage: www.elsevier.com/locate/sna

Development of a piezoelectric-driven miniature pump for biomedical applications

H.K. Ma [a,*], R.H. Chen [a], Y.H. Hsu [b]

[a] Department of Mechanical Engineering, National Taiwan University, Taipei, Taiwan
[b] The Institute of Applied Mechanics, National Taiwan University, Taiwan

ARTICLE INFO

Article history:
Received 5 June 2015
Received in revised form 24 July 2015
Accepted 10 August 2015
Available online 22 August 2015

Keywords:
Miniature pump
Piezoelectric actuator
Biomedical fluid handling

ABSTRACT

Miniature pumping system is widely used in mechanical and bio-medical fields, and in this regard, extensive researches are being conducted in related applications. This paper reports a novel piezoelectric-driven miniature pump that can achieve high flow rate through a combination of piezoelectric-actuator and pumping chamber with internal rib structures. The major features of the proposed miniature pump are self-priming and high flow rate at low frequency range. Flow rates at different frequencies were measured under different piezoelectric-actuator thicknesses and fluid viscosities. In addition, the correlation between the actuator displacement and the pumping efficiency at different frequencies was investigated and discussed. High flow rates of up to 196 ml/min and 141 ml/min were achieved for water and blood mimicking fluid, respectively. It was achieved by using a piezoelectric actuator with a 0.2 mm thick piezoelectric layer and a 0.25 mm thick brass plate, and a pumping chamber with 0.05 mm embedded flow-guiding rib structures for pumping efficiency improvement.

1. Introduction

Miniature pumps are widely used in many fields, including biology, chemistry, medical treatment, and cooling systems. In general, miniature pumps can be categorized into two types, dynamic driven and mechanical displacement. Dynamic pumping, which usually utilizes interactions of fluid with an electric or magnetic field to exert driving forces on the fluid continuously, are typically represented by electro-hydrodynamic [1] and magneto-hydrodynamic [2] pumps. A displacement pump, on the other hand, uses a moving mechanical part to change the volume of a chamber to drive fluid within the chamber. Among various displacement pumps, reciprocating micropumps are typically designed with compact sizes and are thus suitable for integrating with various fluid systems.

Based on actuation mechanisms, the reciprocating micropumps can be categorized as follows—piezoelectric [3], electrostatic [4], pneumatic [5], electromagnetic [6], thermopneumatic [7], shape memory alloy (SMA) [8] and ultrasonic [9]. Among these actuation mechanisms, the piezoelectric-actuators have several advantages, such as large actuation force, short response time, high reliability, simple structure, small size and light weight, and have been widely developed and analyzed in the field of micro-electro-mechanical-systems (MEMS) [10–13]. Various studies have been conducted to investigate the characteristics of piezoelectric-actuated MEMS micropumps. For example, Kim and Jones [14] used a linear strain assumption to predict the optimal rectangular actuator-to-plate thickness ratio at different ratios of Young's modulus. The moment was optimized by a dual-layered piezoelectric actuator. Yoon and Washington [15] proposed a moment balance method to analyze a beam-shape piezoelectric actuator. Luo and Yin [16] designed and fabricated four types of micropumps with different bimorph piezoelectric actuators and check valves. Truong and Nguyen [17,18] presents a lamination technique by designing two micro check valves fabricated by using a 100 μm-thick SU-8 film. A flow rate of 1 to 1.6 ml/min was achieved. Sayar and Farouk [19] developed a piezoelectric valve-less micropump and applied it to transport water. The effects of inlet-outlet port angles and the overall pump size on the flow rate were investigated.

For bio-fluidics and cooling applications, a high flow rate is highly desirable. Cantwell et al. [20] proposed a low-cost, high flow rate electromagnetic micropump, achieving 170 ml/min. Ma et al. [21,22] interfaced one-sided piezoelectric micropumps with a heat-dissipation system and an optimal flow rate of 140 ml/min was achieved with a pump back pressure of 6.4 kPa. Despite of the high flow rate achieved by prior researches, so far there have

* Corresponding author. Fax: +886 2 23632644.
E-mail address: skma@ntu.edu.tw (H.K. Ma).

http://dx.doi.org/10.1016/j.sna.2015.08.003
0924-4247/

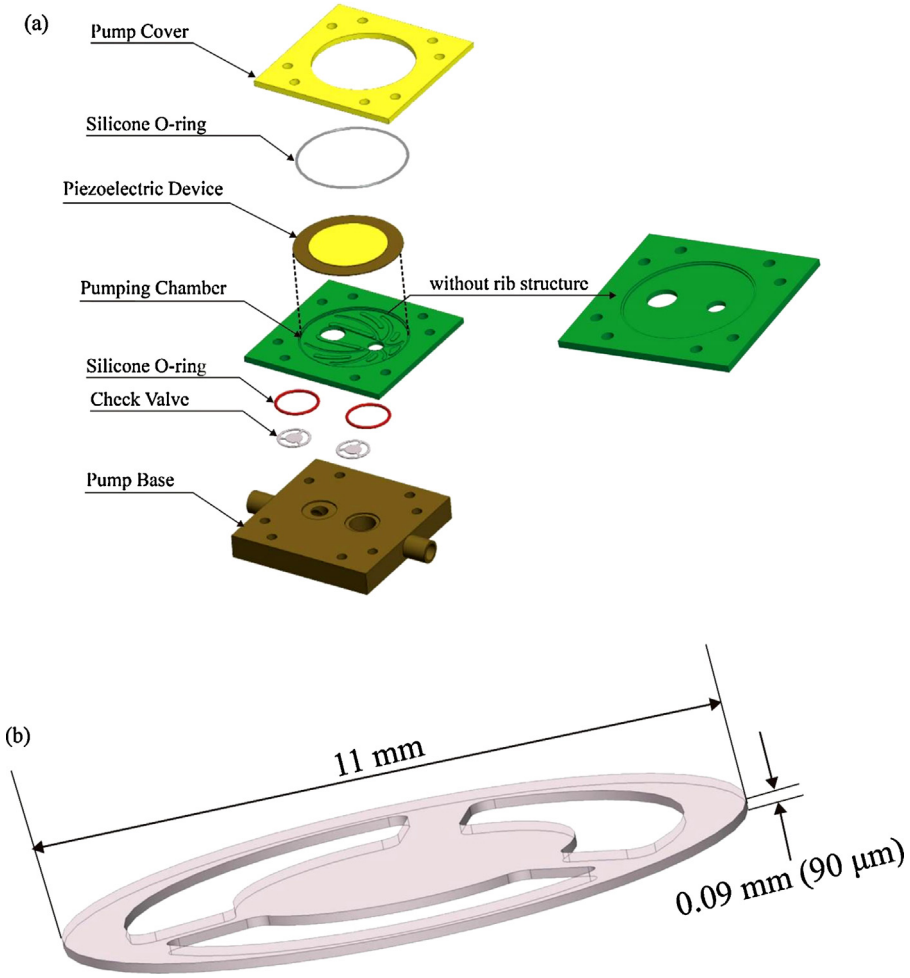

Fig. 1. Structure of (a) the miniature pump assembly (b) the check valve.

been no commercialized, high flow-rate micropumps suitable for integrating with bio-medical or cooling systems.

The aim of the present study is to develop and characterize a high flow rate miniature pump suitable for commercial use in bio-medical and warming/cooling applications. Typical commercially available blood transfer devices have flow rates ranging from 80 ml/min to 200 ml/min. For example, Belmont Buddy® Lite™ AC provides 80 ml/min flow rate, 3 M™ Ranger™ System (model 245) has a standard flow rate of 150 ml/min, and GE Healthcare enFlow system offers a standard flow rate is 200 ml/min. Our proposed miniature pumps can meet the standard flow rate for this kind of blood transfer applications. For the biomedical applications, a circular chamber structure was chosen to achieve easy assembly of the miniature pumps. Both water and blood-mimicking fluid were used to investigate the influence of fluid viscosity on flow rate. To optimize the performance of the miniature pump, a series of rib structures were designed based on flow-field simulation within the miniature pump chamber and the effects of the rib structures on the flow rate were also investigated. Three types of miniature pumps with different chamber structures and piezoelectric-actuator thicknesses were designed, fabricated and measured at different frequencies. The miniature pump performance was evaluated and discussed based on the measured flow rates under different pumping structures and settings.

2. Development of the piezoelectric-driven pump

2.1. Miniature pump structure and flow mechanism design

The basic structure of the circular piezoelectric miniature pump is shown in Fig. 1(a). The external dimension of the pump is 50 mm × 50 mm × 12 mm. The case of the miniature pump was made by machining a Poly-methyl-methacrylate (PMMA) block with a computer numerical controlled (CNC) milling machine. Commercially available piezoelectric coated brass disks were used in this study. Lead zirconate titanate (PZT) was used to serve as the piezoelectric layer. Two check valves were made out of a 0.09 mm thick silicone film, and it was cut out by using a Nd:YAG laser cutting machine. The assembly was done by placing all pieces together layer-by-layer and then clamped together with 4 screws and silicone O-rings between layers. The space between the piezoelectric actuator and the lower case formed the miniature pump chamber, with a diameter of 34 mm and a chamber depth d = 0.45 mm. A circular piezoelectric-actuator with a diameter of 35 mm covered the chamber to form a tight seal. This piezoelectric-actuator drove fluids in and out the chamber through check valves fabricated on the lower case. To further optimize the flow rate, a series of rib structures were designed within the chamber. Fig. 2 shows different rib structure designs within the chamber. The gap p, defined as the space between the piezoelectric-actuator and the rib structure, was one key feature of the rib structure design. Two types

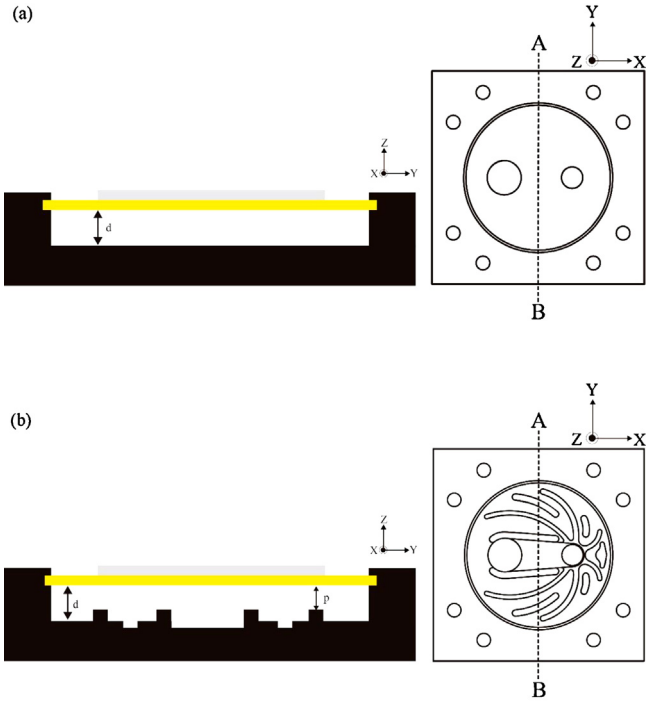

Fig. 2. Pumping chamber cross-section view (along the A–B line from the top view) (a) without rib structures (b) with rib structures.

of rib heights, 0.05 mm and 0.25 mm, were chosen to form two different gaps $p = 0.4$ mm and 0.2 mm. For simplicity in construction and high rigidity, bridge type valves were adopted as the design for the check valves in the piezoelectric miniature pump (Fig. 1(b)). The actuation of the check valves were coupled to the oscillation of circular piezoelectric-actuator through the chamber pressure change caused by the actuator displacement.

Fig. 3 shows the pumping mechanism of the miniature pump. The voltage-driven oscillation of the piezoelectric-actuator produces a displacement. The displacement changes the pressure within the chamber and thus causes the check valves to move. As the piezoelectric-actuator moves downward, the increased inner pressure makes the inlet valve close and the outlet valve open, leading to an outflow toward right. As the actuator moves upward, the inner pressure decreases and makes the inlet valve open and the outlet valve closed, leading to an inflow toward left.

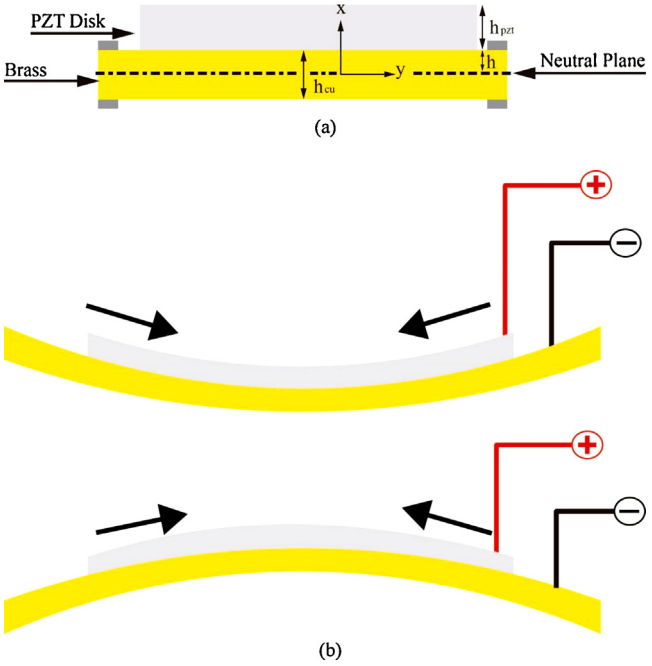

Fig. 4. Brass-based piezoelectric actuator: (a) schematic view (b) activated by AC voltage.

2.2. Design of the piezoelectric-actuator

Fig. 4(a) shows the schematics of the piezoelectric-actuator, formed by binding piezoelectric material with a brass diaphragm plate. When driving voltage was applied to the piezoelectric layer, the piezoelectric layer started oscillating, causing the brass diaphragm to move. To ensure a vertical movement of the diaphragm, the radius of the piezoelectric layer should be smaller than the brass diaphragm radius. The thicknesses of the piezoelectric layer and the brass diaphragm affect the displacement of the entire actuator. In Fig. 4(a), there exists a neutral plane with zero momentum and zero the shear stress. The location of this neutral plane can be determined by solving the Governing Equation. The following equation can be deducted to represent the principle:

$$\Sigma F_x = 0 = \int \sigma_x dA \tag{1}$$

$$\int_{-h}^{-(h-h_{cu})} \sigma_{cu} dA + \int_{-(h-h_{cu})}^{0} \sigma_{pzt} dA + \int_{0}^{-(h+h_{cu})+h_{pzt}} \sigma_{pzt} dA = 0 \tag{2}$$

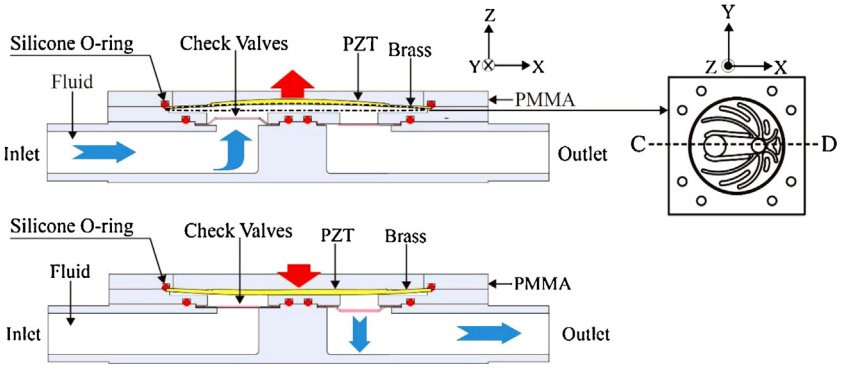

Fig. 3. Schematic view of the pumping operation (cross-section C–D).

From (2), the location of neutral plane can be found, as shown in (3)

$$h = \frac{\left[\left(1-\nu_{pzt}^2\right)\left(E_{Cu}h_{cu}^2\right)+\left(2E_{Pzt}h_{Cu}h_{Pzt}+E_{pzt}h_{pzt}^2\right)\left(1-\nu_{cu}^2\right)\right]}{2\left[\left(E_{cu}h_{cu}\right)\left(1-\nu_{pzt}^2\right)+\left(E_{pzt}h_{pzt}\right)\left(1-\nu_{cu}^2\right)\right]} \tag{3}$$

where E_{cu} and E_{pzt} represent the Young' modulus of the brass diaphragm and the piezoelectric (PZT) layer, respectively, ν_{cu} and ν_{pzt} are the Poisson ratios, h_{cu} is the thickness of the brass disk, h_{pzt} is the piezoelectric layer thickness, and h is the distance between the neutral surface and the bottom of the piezoelectric layer.

Referring to Fig. 4(b), a periodically varying sinusoidal electric field is generated within the piezoelectric layer via the electrical contacts on the piezoelectric layer and the brass plate. The varying electric field causes the piezoelectric actuator to bend periodically, and therefore pumps the fluid flow through the system with the coordination with the bridge valves. As long as the pumping force can overcome the fluidic resistance, inertia and viscosity, the pumping flow can be directed effectively. To understand the performance of the miniature pump at different pumping frequencies, the bending vibration of the piezoelectric actuator was theoretically derived [23] as follows. For a bending plate, the linear strain distribution conditions are

$$\epsilon(Z) = \epsilon_{pzt} = \epsilon_{cu} = Z\kappa \tag{4}$$

$$\sigma_{cu} = \frac{E_{cu}Z}{1-\nu_{Cu}^2} \tag{5}$$

where ϵ_{pzt} is the strain of the PZT-actuator, ϵ_{cu} is the strain of the brass plate, κ is the radius of curvature of bending plate, σ_{cu} refers to the stress at the interface between the piezoelectric layer and the brass plate, Z is the deflection displacement of the neutral surface. From the liner piezoelectric constitutive equations [21], the stress and strain relationship for the PZT-actuator can be expressed as

$$\sigma_{pzt} = \frac{E_{pzt}Z}{1-\nu_{pzt}^2}\left(\kappa Z - \frac{Vd_{31}}{h_{pzt}}\right) = \frac{E_{pzt}\kappa Z^2}{1-\nu_{pzt}^2} - \frac{E_{pzt}Vd_{31}Z}{h_{pzt}\left(1-\nu_{pzt}^2\right)} \tag{6}$$

where d_{31} is the electrical–mechanical coupling coefficient in the z-direction and V is the applied voltage. Furthermore, the moment balancing equations of the bending structure gives

$$M = -\int_{-h}^{h_{Cu}-h}\sigma_{cu}Z_{cu}dz - \int_{h_{Cu}-h}^{0}\sigma_{pzt}Z_{pzt}dz - \int_{0}^{h_{Cu}-h+h_{pzt}}\sigma_{pzt}Z_{pzt}dz \tag{7}$$

$$= -\int_{-h}^{h_{Cu}-h}\frac{E_{Cu}}{1-\nu_{Cu}^2}z_{cu}^2dz - \int_{h_{cu}-h}^{h_{cu}-h+h_{pzt}}\left(\frac{E_{pzt}Z_{pzt}}{1-\nu_{pzt}^2} - \frac{E_{pzt}Vd_{31}}{h_{pzt}\left(1-\nu_{pzt}^2\right)}\right)Z_{pzt}dz = 0 \tag{8}$$

Table 1
Pump component parameters.

Piezoelectric actuator parameters	Value
Piezoelectric layer Young's modulus, E_{pzt} (GPa)	52
Piezoelectric layer Poisson's ratio, ν_{pzt}	0.31
Piezoelectric layer d_{31} (m/v)	-2.10×10^{-10}
Piezoelectric layer density (kg/m^3)	7.78
Brass plate Young's modulus, E_{cu} (GPa)	103
Brass plate Poisson's ratio, ν_{cu}	0.33
Silicon check valve density (kg/m^3)	1800
Silicon check valve Young's modulus, E_{si} (MPa)	25.5
Silicon check valve Poisson's ratio, ν_{si}	0.48

Eq. (7) and (8) can be further deduced to

$$M = \frac{E_{pzt}Vd_{31}\left(h_{pzt}+2h_{cu}-2h\right)}{2\left(1-\nu_{pzt}^2\right)} = \left[\frac{E_{Cu}I_{cu}}{3\left(1-\nu_{cu}^2\right)} + \frac{E_{pzt}I_{pzt}}{3\left(1-\nu_{pzt}^2\right)}\right]\kappa \tag{9}$$

The piezoelectric moment M can be calculated by using the parameters provided by PZT vendors (listed in Table 1) and substituting them into Eq. (9). Table 2 lists the neutral plane position h and piezoelectric moment thickness M under different piezoelectric layer thickness, calculated from Eq. (5) through (9). It can be seen that as the thickness of the piezoelectric layer decreases, the position of the neutral plane h shifts towards the piezoelectric layer, the piezoelectric moment M decreases, but the curvature radius κ increases.

2.3. Design of rib structures within the chamber

In order to understand the contribution of rib structures, finite element simulation was performed (with working fluid parameters shown in Table 3) to estimate the flow resistance and the resulting flow field under a predetermined pressure drop applied between a lateral inlet and a lateral outlet as shown in Fig. 3. A three-dimensional steady-state model of the miniature pump chamber was developed with the "gap", p, the vertical space between the rib structure and the chamber top, as the main variable. The simulation model was implemented using ANSYS Fluent. The Navier-Stokes equations were applied as the governing equations. SIMPLEC algorithm was used for pressure-velocity coupling, and the second-order upwind method was used for discretizing equation. The gap p changed from 0.45 mm to 0.1 mm, in accordance with the change in height of the rib structure from 0 mm to 0.35 mm. The assumptions for the simulation model are listed as follows:

(1) Laminar flow for single phase incompressible liquid.
(2) Three-dimensional steady flow.
(3) Inlet boundary condition: constant pressure (100 Pa).
(4) Outlet boundary condition: constant pressure (0 Pa).
(5) Contribution from gravity is ignored.
(6) Non-slippery wall.
(7) Smooth triangle mesh of 20,994,227 elements.
(8) Iteration limit: dimensionless residuals reaching 10^{-5}.

Table 2
Theoretical calculation of PZT deflection properties for different piezoelectric thickness.

Experimental condition	Thickness (mm)	Neutral Plane	Moment	Kappa
Piezoelectric	0.1	1.54×10^{-4}	2.47×10^{-1}	5.3×10^{-1}
	0.2	1.89×10^{-4}	2.72×10^{-1}	4.5×10^{-1}
	0.3	2.28×10^{-4}	2.91×10^{-1}	2.8×10^{-1}
	0.4	2.69×10^{-4}	3.06×10^{-1}	1.6×10^{-1}
Brass	0.25			

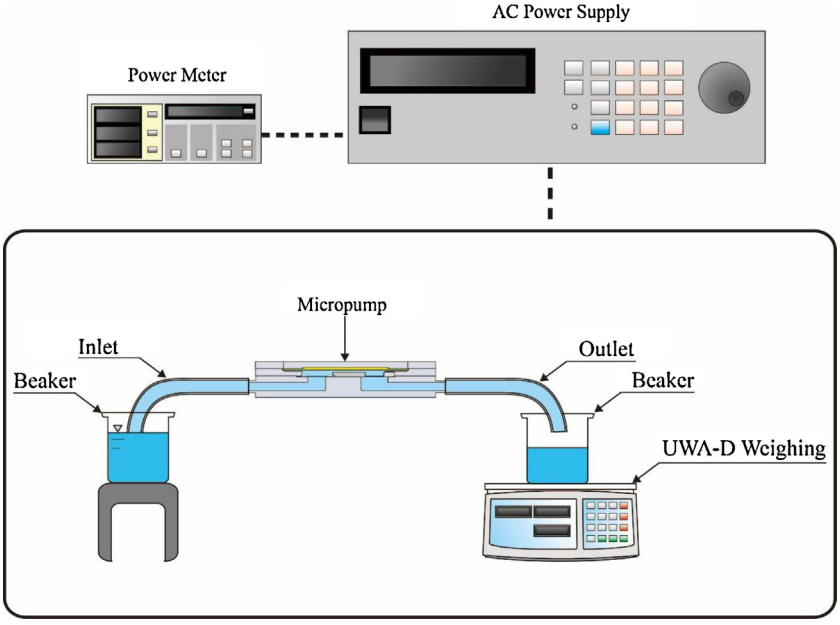

Fig. 5. Experimental setup.

Table 3
Parameters for the flow field simulation.

	Fluid	Density (kg/m^3)	Viscosity (kg/m)
Working fluid	Water	1000	0.0014
	Blood mimicking	1050	0.004
Chamber gap	0.1~0.45 mm with 0.05 mm step		

3. Experimental setup

As shown in Fig. 5, the proposed high flow rate miniature pump was driven by a sinusoidal alternating-current (AC) signal generated from Chroma 61,501 AC Source and amplified to ±70 V by the Power meter Chroma 66,201. The inlet and outlet of the two pipes were leveled to create a 0 Pa backpressure in our system. An MTI-2100 fiber-optic measurement instrument was used to measure the maximum displacement of the piezoelectric actuator. The flow rate was quantified by measuring the average increase of total liquid weight (UWA-D). The flow rates were recorded to analyze the pump performance at different input frequencies. The measurement was performed at the driving frequency changing from 15 Hz to 110 Hz at a 5 Hz step. Miniature pumps with different parameters, such as piezoelectric thickness, rib structure and working fluid were fabricated for these experiments. The results have been discussed in the following section.

4. Results and discussion

This section reports the measured properties of the proposed miniature pump with a high flow rate. The measurement results were divided into three parts to organize the discussion

4.1. The contribution of piezoelectric actuator performance to pump efficiency

The flow of the piezoelectric miniature pump was initiated by the volume change caused by the deflection of the piezoelectric actuator. Therefore, the design of the piezoelectric actuator has a great influence on its basic performance. According to Eqs. (3) and (9), it can be realized that κ, which represents amplitude of

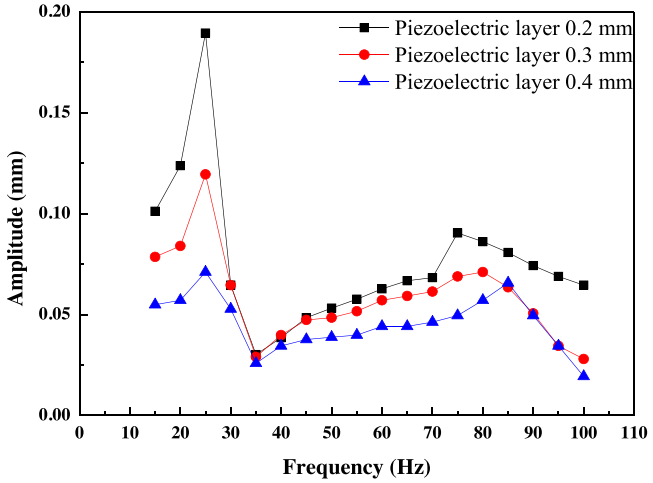

Fig. 6. Deflection amplitude of the piezoelectric actuator with different piezoelectric layer thickness (driving voltage: ±70 V).

the piezoelectric actuator, changes with different thicknesses of the piezoelectric layer, as shown in Table 2. To further verify the theoretical calculation shown in Section 2, MTI-2100 fiber-optic measurement was done to obtain the maximum deflection amplitudes of the piezoelectric actuators with different piezoelectric layer thicknesses, within the series of fabricated micorpumps, using water as the pumping fluid. The thicknesses of piezoelectric layers in the fabricated miniature pumps were 0.2 mm, 0.3 mm, and 0.4 mm. Fig. 6 shows the fiber-optic measurement results. It can be found that the piezoelectric actuator with 0.2 mm thick piezoelectric layer displayed the largest deflection amplitude over 15–100 Hz frequency range in agreement with the theoretical calculation. The maximum actuator deflection amplitude of 0.19 mm was reached at a low vibrating frequency of 25 Hz. Fig. 7 further shows the water flow rate measurement results of these miniature pumps in the frequency range of 15–100 Hz. The close similarity between the flow rate change and the deflection amplitude change in the 15–100 Hz frequency range suggested that the flow rate was highly related to

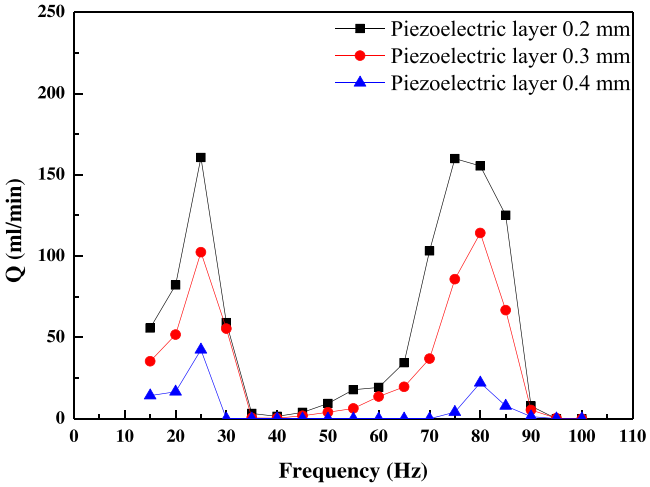

Fig. 7. Flow rates of miniature pumps with different piezoelectric layer thickness (Driving voltage: ±70 V).

the deflection amplitude of the actuator. The miniature pump with 0.2 mm piezoelectric layer indeed produced a higher flow rate than the miniature pumps with other piezoelectric layer thicknesses.

The resonance frequency is one key characteristic of the proposed miniature pump. As shown in Fig. 6, for the miniature pump with 0.2 mm piezoelectric layer, the deflection amplitude of the piezoelectric actuator showed two peaks at 25 Hz and 75 Hz, suggesting that these two frequencies were the base frequency and the third octave frequency, respectively. Fig. 6 also shows that the resonance frequency shifted to higher values as the thickness of the piezoelectric layer increased. On the other hand, the pumping efficiency of the miniature pump was not totally determined by the deflection amplitude of the piezoelectric actuator. For the miniature pump with 0.2 mm piezoelectric layer, the measured flow rates in Fig. 7 are 161 ml/min and 160 ml/min at 25 Hz and 75 Hz, respectively, while the deflection amplitudes shown in Fig. 6 are 0.19 mm and 0.09 mm at 25 Hz and 75 Hz, respectively, with water in the pumping chamber.

To identify the peaks of high flow rate found in the experimental result, we used an Agilent 4294A Precision Impedance analyzer to measure the resonant modes of the piezoelectric actuator. Because of the experimental environment, the pipes installed at the inlet and outlets were shortened from 20 cm to 5 cm. Since the lowest measurable frequency of Agilent 4294A was 40 Hz, we use it to study the frequency response of the miniature pump found at 75 Hz. Fig. 8(a) and (b) shows the measured frequency responses of the clamped piezoelectric disk and after it embedded into the piezoelectric miniature pump, respectively. In Fig. 8(a), it shows that edge-clamped piezoelectric disk has it first resonance frequency at 1.5 kHz. After assembly and filled with water into the chamber, multiple additional resonant peaks were identified at 65 Hz, 202 Hz, 856 Hz. The original first resonant peak of the clamped piezoelectric disk moved from 1.5 kHz to 1.9k Hz with a higher damping ratio. Note that there is a resonant peak found at 65 Hz, which was close to the resonant peak found in the experimental result shown in Fig. 8(a). A higher resolution scanned is also shown in Fig. 8(b). This experimental result demonstrated that additional resonant model could be introduced by the designed piezoelectric miniature pump. They played an important role to generate a high flow rate in the piezoelectric miniature pump. Note that the measured frequency (65 Hz) was lower than the experimental data (75 Hz), it was due to the pipes connected to the inlet and outlet was shortened and cause the resonant frequency shifted.

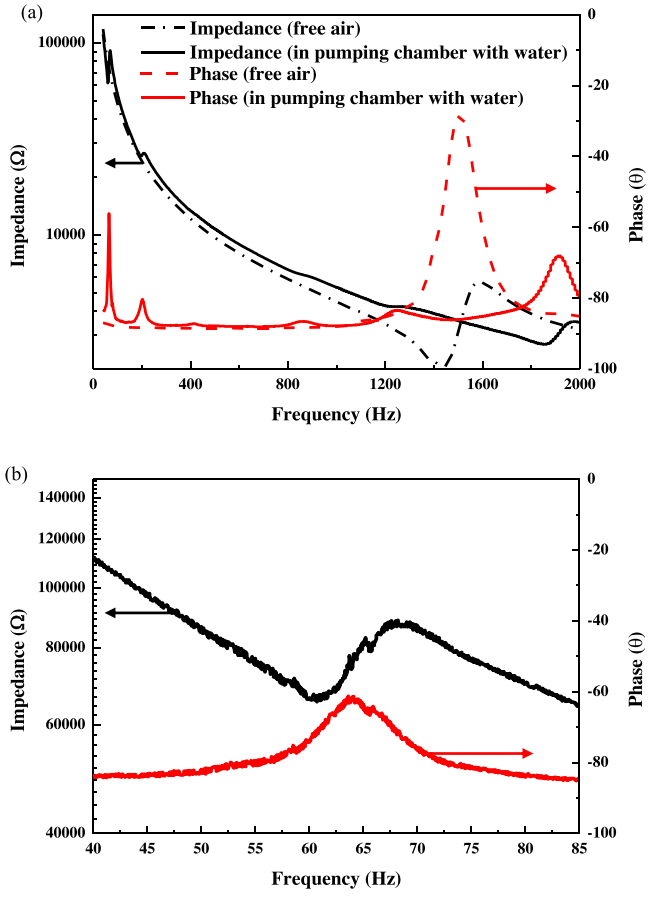

Fig. 8. Impedance responses of (a) clamped piezoelectric disk (black dashed line: Impedance; red dashed line: phase) and embedded it into the miniature pump (black line: Impedance; red line: phase), and (b) the impedance response of the whole system near the first resonant peak.

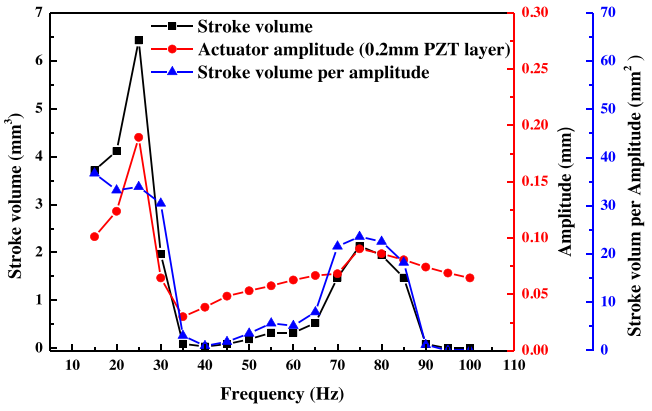

Fig. 9. Frequency response of miniature pumps under the case of chamber gap $p = 0.45$ mm without rib structure with water. (For interpretation of the references to color in the text, the reader is referred to the web version of this article.)

To further verify this effect, as shown in Fig. 9, we calculated the stroke volume per unit amplitude of each cycle from 15 Hz to 100 Hz (blue line). It was done by dividing the stroke volume (black line) by the measured actuator vibrating amplitude (red line) and the corresponding frequency. The stroke volume was calculated by dividing measured volume flow rate with respect to operating frequency. The stroke volume per unit amplitude represents the level of the phase difference between the vibration of the

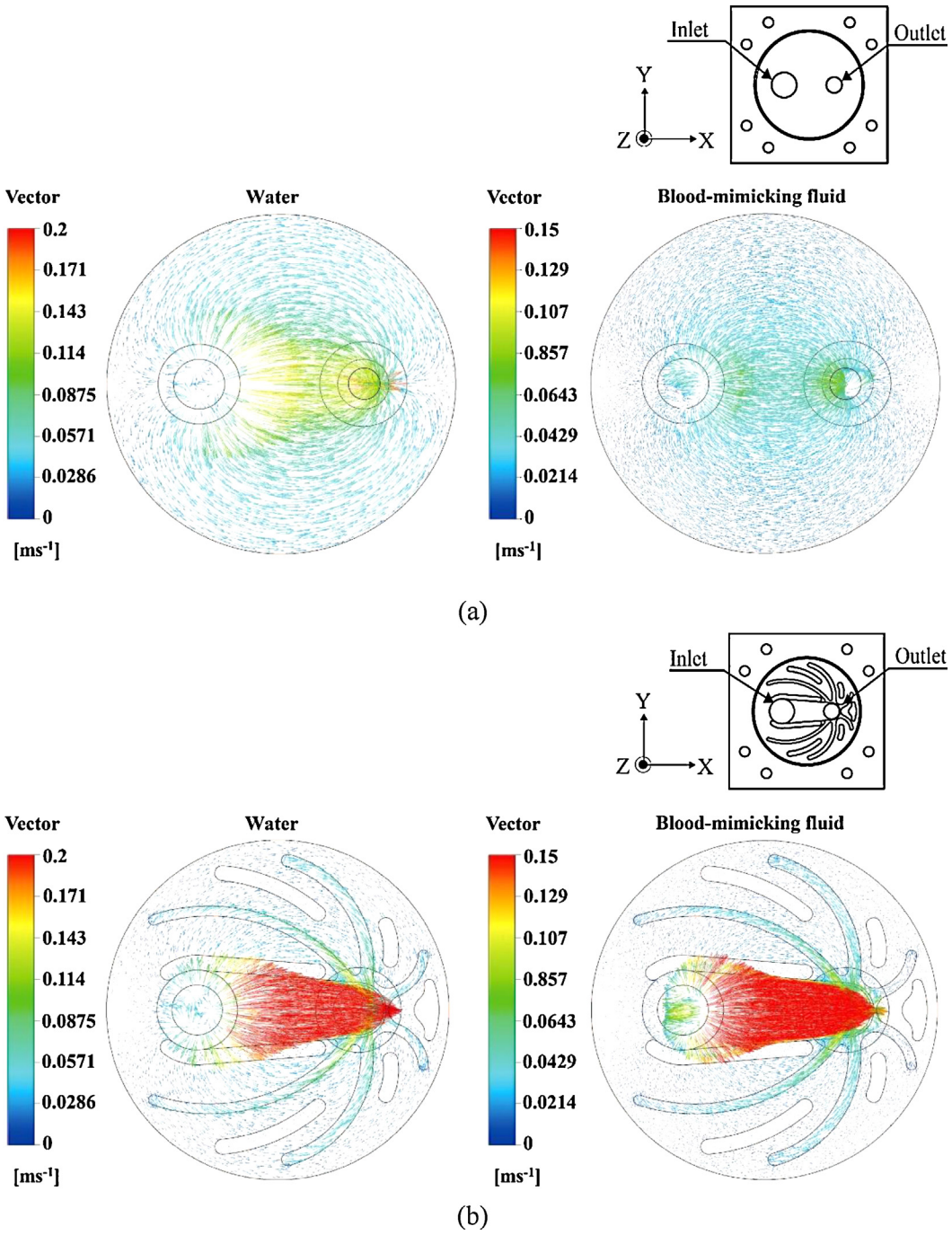

Fig. 10. Comparison of flow field simulation results (top view) for water and blood-mimicking fluid (a) chamber without rib structures (b) chamber with rib structures.

actuator and the vibration of the check valves for each pumping cycle. A higher value means the actuator and the valves are vibrating more "in-phase", and vice versa. It can be clearly observed from Fig. 9 that in the frequency ranges of 15–30 Hz and 70–85 Hz, the stroke volume per unit volume is higher. It suggests that the vibration of the actuator and valves has less phase difference. On the contrary, between the two resonant frequencies (30–70 Hz), the stroke volume per unit amplitude is very low, suggesting that the actuator and the valves are moving nearly out of phase. It causes an extremely low pumping efficiency. Further, a relative flat stroke volume per unit amplitude was found at and around the two highest flow rate regions. It implies that the piezoelectric miniature pump must go into a resonant state and a high flow rate can be achieved at low frequency.

4.2. Finite element study on the effect of the ribs structure

4.2.1. Flow fields in chambers with and without rib structures

During the miniature pump operation, the fluid was assumed to flow from the inlet to the outlet. However, in a circular chamber without any restriction, longer flow paths extended to the rim of the chamber might be formed and reduce the pumping efficiency. The simulation was conducted in two steps. First, flow in a circular chamber without rib structure was simulated to study the "free" flow field within the chamber. Second, the flow field was simulated with rib structures aligned with the flow pattern added to the chamber. The results of this two-step simulation are shown in Fig. 10(a) and (b), respectively. It can be clearly seen that the rib structures can effectively confine the flow in the shortest path

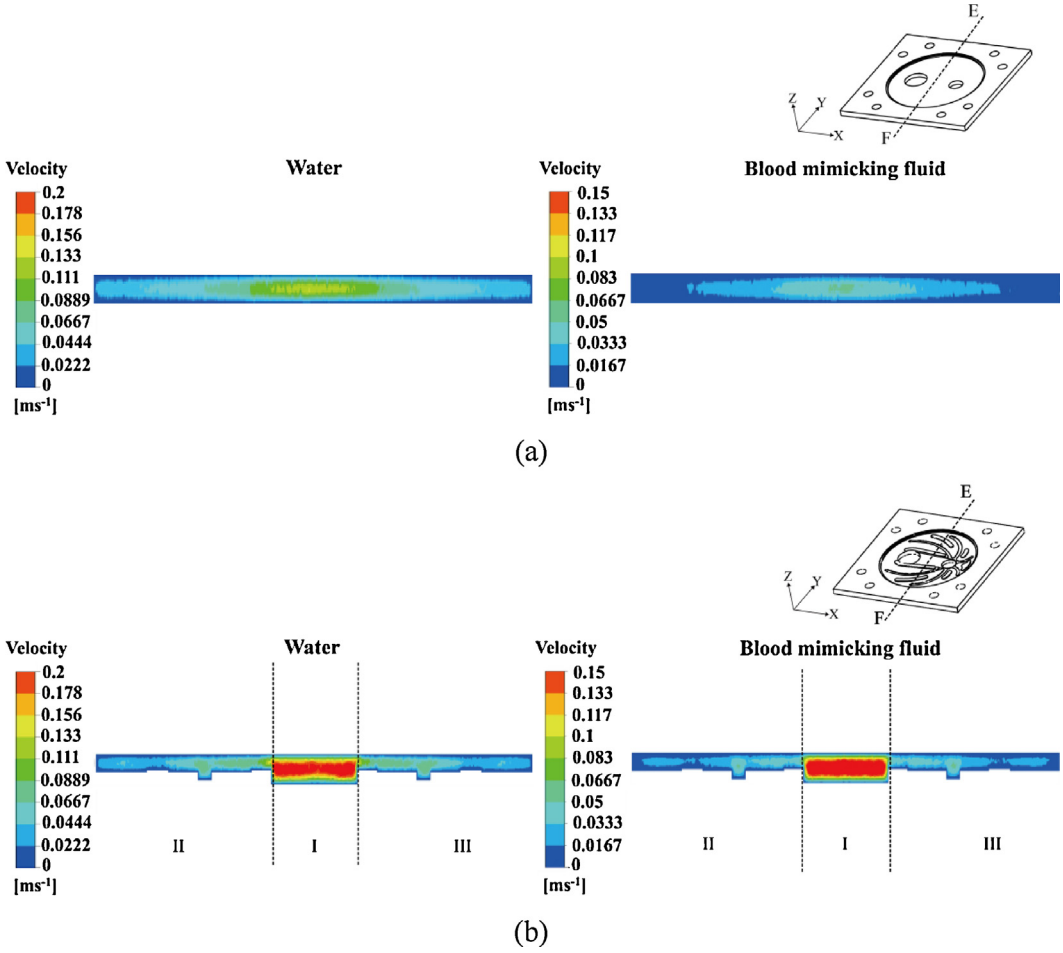

Fig. 11. Comparison of flow field simulation results (cross-section E–F) for water and blood-mimicking fluid with different pumping chamber structure: (a) chamber without rib structures (b) chamber with rib structures.

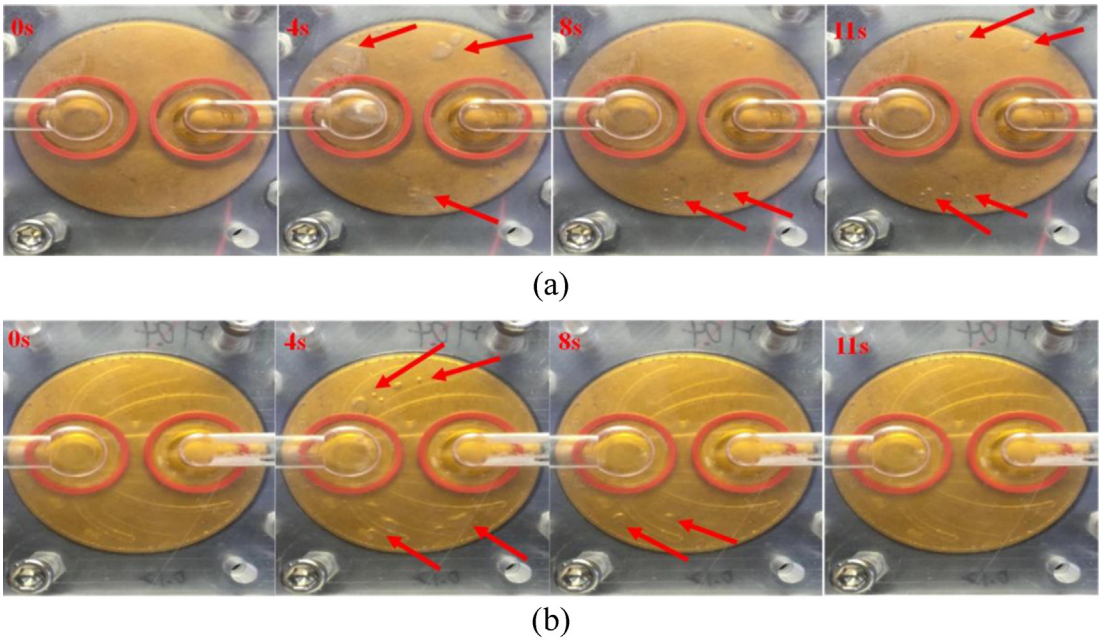

Fig. 12. Bubble distribution within the pumping chamber (outlet at left): (a) chamber without rib structures (b) chamber with rib structures.

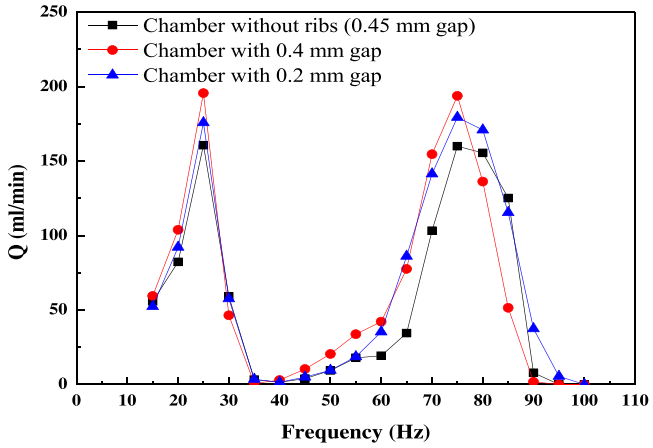

Fig. 13. Flow rates of miniature pumps with different gap spaces within the chamber for water (driving voltage: ±70 V).

between the inlet and the outlet. Fig. 11 further reveals a highly concentrated flow between the rib structures in the cross-section view of the chamber space between the inlet and the outlet.

To further verify the results of the simulation, bubbles were pumped into the chamber and continuous photos were taken to trace the flow path of the working fluid (water). As shown in Fig. 12(b), bubbles were effectively confined between the rib structures. Moreover, the randomly moving bubbles in the chamber without rib structures (shown in Fig. 12(a)) had higher chances to stay inside the chamber, making the miniature pump unstable. Therefore, the design of the rib structures may also improve the bubble tolerability and thus the reliability of the miniature pump.

4.2.2. *Effects of gap height*

Since the rib structures were proven to have positive effects on flow rate enhancement, it is necessary to determine the influence of the rib height on the flow efficiency. In Fig. 13, three miniature pumps with different rib structure heights were fabricated and the flow rates were measured. The fabrication variable was the gap p (p = 0.45 mm, 0.4 mm, and 0.2 mm in Fig. 13), the distance between the lower edge of the piezoelectric actuator and the top of the rib structure, with the fixed chamber depth d = 0.45 mm. The flow rate comparison in Fig. 13 suggests that the miniature pump with p = 0.4 mm had a higher flow rate than the pump with p = 0.2 mm and the pump without rib structures (p = 0.45 mm).

The highest flow rate was observed for p = 0.4 mm miniature pump (196 ml/min at 25 Hz and 194 ml/min at 75 Hz). There was a large 21% yet consistent increase from the flow rate of the miniature pump without ribs (161 ml/min at 25 Hz and 160 ml/min at 75 Hz). On the other hand, the p = 0.2 mm miniature pump showed a moderate 10% flow rate increase from the miniature pump without rib structures, and the flow rate increase was smaller than that of the miniature pump with p = 0.4 mm. This flow rate difference possibly arose due to the differences in the rib structure heights. The p = 0.2 mm miniature pump had a 0.25 mm high rib structure, which was more than half of the chamber depth of 0.45 mm and probably caused additional flow resistance within the chamber.

In Fig. 11, simulated flow field at the cross-sectional plane (E–F) shown in the inset is plotted for both pumping chamber without (Fig. 11(a)) and with (Fig. 11(b)) rib structures. Different from pumping chamber without rib structures, the flow paths at edge pumping chamber with rib structures were narrowed, causing an increase of flow resistance (60% increase on regions II and III for 0.05 mm rib). This higher flow resistance force fluid to flow into and concentrate at the central region I. By taking the shortest path in the center groove, the overall flow rate can be increased

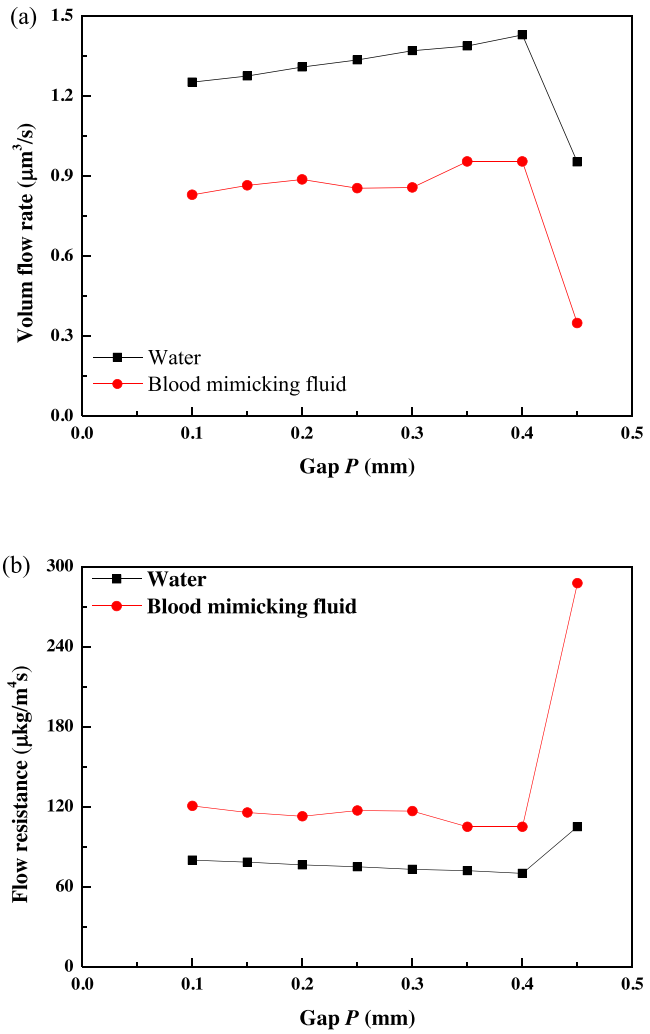

Fig. 14. Simulation results of (a) volume flow rate (b) flow resistance within chambers with different gap spaces.

significantly. This can be further verified by calculating volume flow rates from the simulated results shown in Fig. 11(b). Fig. 14(a) and (b) show the calculated results based on the following general equation of flow resistance based on the Hagen-Poiseuille law [24]:

$$R_{hyd} = \frac{\Delta P}{Q} \tag{10}$$

where R_{hyd} is the flow resistance, ΔP is the pressure drop across the inlet and outlet, Q is a volume flow rate shown in Fig. 14(a). In Fig. 14(a), we demonstrated that using 0.05 mm high rib structures (gap p = 0.4 mm) can immediately increase the volume flow rate to 50% more.

4.3. *Effects of different working fluids*

In addition to the application of the miniature pumps in infusion jet, this study intended to investigate the potential application of the miniature pumps in biomedical infusion by using a blood-mimicking fluid with higher viscosity than water. Fig. 15 compares the flow rates of miniature pumps with different gap spaces for both water and the blood-mimicking fluid. The flow rate sharply decreased by 28–38% for miniature pumps with different chamber gap structures as the working fluid was changed from water to the blood-mimicking fluid with higher viscosity. The miniature pump with p = 0.4 mm gap space (0.05 rib height) exhibited

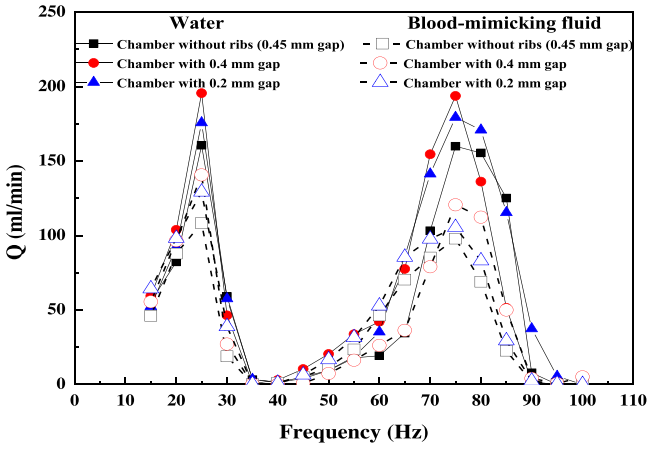

Fig. 15. Flow rate comparison between water and blood-mimicking fluid for miniature pumps with different gap spaces within the chamber (Driving voltage: ±70 V).

the highest flow rates of 141 ml/min at 25 Hz and 125 ml/min at 75 Hz for the blood-mimicking fluid, consistent with the simulation result shown in Fig. 14. This suggested that the rib structures also have flow concentrating effect on blood-mimicking fluid. Compared with the flow rates of 196 ml/min at 25 Hz and 194 ml/min at 75 Hz for water, the increased fluid viscosity caused a decrease in the flow rate, via 28% at 25 Hz and 36% at 75 Hz. This signified that an increase in viscosity reduces the pumping efficiency at 75 Hz. Therefore, for application in biomedical infusion, a lower pumping frequency is preferred.

5. Conclusions

The current study has proposed a high flow rate piezoelectric-actuated miniature pump with flow-concentrating rib structures deployed inside the pumping chamber. A series of miniature pumps made of PMMA with different brass-based piezoelectric-actuators and rib structures were fabricated and tested for flow rates. Simulations were also performed to verify with the experimental results. The major conclusions are as follows:

1. For the brass-based piezoelectric actuator, the piezoelectric layer thickness shows strong influence on the amplitude of deflection. A thinner piezoelectric layer can result in a higher deflection. For fabricated piezoelectric actuators, the 0.2 mm thick piezoelectric layer gives the largest deflection amplitude of 0.19 mm when pumping water.
2. The fabricated miniature pumps show two resonant frequencies in the range of 15–100 Hz. For the miniature pump with 0.2 mm piezoelectric layer, the water flow rate can reach up to 161 ml/min as the base frequency of 25 Hz; on the other hand, under the third-octave frequency of 75 Hz, the water flow rate is 160 ml/min.
3. Rib structures deployed within the pumping chamber show strong flow guiding effect between the inlet and the outlet inside the chamber and positively increase the water flow rate by 20%. Increasing the height of the rib structures, however, has a negative effect the water flow rate, possibly due to the increased flow resistance inside the chamber.
4. For biomedical infusion applications, blood-mimicking fluid with higher viscosity was tested. The characteristic flow response of the blood-mimicking fluid to the piezoelectric layer thickness and the rib structures remain similar to that of water. The high viscosity reduces the pumping efficiency, it cause the maximum flow rate decrease 28% than water, but a lot more at higher frequency (~75 Hz). It suggested that a lower driving frequency (~25 Hz) worked better for biomedical infusion applications.

Acknowledgment

This research was funded by the Ministry of Economic Affairs, R.O.C. (103-EC-17-A-19-S1-225).

Appendix A. Supplementary data

Supplementary data associated with this article can be found, in the online version, at http://dx.doi.org/10.1016/j.sna.2015.08.003.

References

[1] E.G. Kim, J.G. Oh, B. Choi, A study on the development of a continuous peristaltic micropump using magnetic fluids, Sens. Actuate. A-Phys. 128 (2006) 43–51.
[2] H. Moritz, M. Stubbe, J. Gimsa, Ac-field-induced fluid pumping in microsystems with asymmetric temperature gradients, Phys. Rev. Lett. 79 (2) (2009) 1–10.
[3] L.C. Wu, C.J. Yang, C.Y. Chen, Low power consumption PZT actuated micropump, in: Proc. IEEE IMPACT, Taiwan, 2006, pp. 65–68.
[4] M.T. Mir, A.S. Ebrahim, Design and simulation of a novel electrostatic peristaltic micromachined pump for drug delivery applications, Sens. Actuate. A-Phys. 117 (2005) 222–229.
[5] E. Meng, X.Q. Wang, H. Mak, Y.C. Tai, A Chech-valved silicon diaphragm pump, in: Proc. 13th IEEE MEMS, Japan, 2000, pp. 23–27.
[6] S.M. Lee, Y.D. Kuan, M.F. Sung, Design and fabrication of a magnetic fluid micro-pump for applications in direct methanol fuel cells, J. Power Sources 196 (2011) 7609–7615.
[7] O.C. Jeong, S. Konishi, Fabrication and drive test of pneumatic PDMS micropump, Sens. Actuate. A-Phys. 135 (2007) 849–856.
[8] D. Xu, L. Wang, G.F. Ding, Y. Zhou, A.B. Yu, B.H. Cai, Characteristics and fabrication of NiTi/Si membrane micropump, Sens. Actuate. A-Phys. 93 (2001) 87–92.
[9] N.T. Nguyen, A.H. Meng, J. Black, R.M. White, Integrated flow sensor for in-situ measurement and control of acoustic streaming in flexural plate wave micro pumps, Sens. Actuate. A-Phys. 79 (2000) 115–121.
[10] C.Y.K. Chee, L. Tong, G.P. Steven, A review on the modeling of piezoelectric sensors and actuators incorporated in intelligent structures, J. Intell. Mater. Syst. Struct. 9 (1998) 3–19.
[11] E. Stemme, G. Stemme, A valve-less diffuser/nozzle based fluid pump, Sens. Actuate. A-Phys. 39 (1993) 159–167.
[12] D.L. DeVoe, A.P. Pisano, Modeling and optimal design of piezoelectric cantilever microactuators, J. Microelectromech. Syst. 6 (1997) 266–270.
[13] C.J. Morris, F.K. Forster, Optimization of a circular piezoelectric bimorph for a micropump driver, J. Micromech. Microeng. 10 (2000) 459–465.
[14] S.J. Kim, J.D. Jones, Optimal design of piezoactuators for active noise and vibration control, AIAA J. 29 (1991) 2047–2053.
[15] H.S. Yoon, G. Washington, Piezoceramic actuated aperture antennae, Smart Mater. Struct. 7 (1998) 537–542.
[16] Y. Luo, X. Yin, Z. Zhang, Vibration performances of polymeric micropump actuated by PbZrTiO3 bimorph, Micro Nano Lett. 10 (2013) 559–562.
[17] T.Q. Truong, N.T. Nguyen, A polymeric piezoelectric micropump based on lamination technology, J. Micromech. Microeng. 14 (2004) 632–638.
[18] N.T. Nguyen, T.Q. Truong, A fully polymeric micropump with piezoelectric actuator, Sens. Actuate. B-Chem. 97 (2004) 137–143.
[19] E. Sayar, B. Farouk, Dynamic analysis of bulk acoustic wave piezoelectric micropumps: effects of inlet-outlet port angles and overall pump size, in: Proc. IEEE IMECE, USA, 2013, pp. 15–21.
[20] M.L. Cantwell, F. Amirouche, J. Citerin, Low-cost high performance disposable micropump for fluidic delivery applications, Sens. Actuate. A-Phys. 168 (2011) 187–194.
[21] H.K. Ma, B.R. Hou, C.Y. Lin, J.J. Gao, The improved performance of one-side actuating diaphragm micropump for a liquid cooling system, Int. Commun. Heat Mass Transf. 35 (2008) 957–966.
[22] H.K. Ma, B.R. Chen, C.Y. Lin, J.J. Gao, Development of an OAPCP-micropump liquid cooling system in a laptop, Int. Commun. Heat Mass Transf 36 (2009) 225–232.
[23] S. Li, S. Chen, Analytical analysis of a circular PZT actuator for valveless micropumps, Sens. Actuate. A-Phys. 104 (2003) 151–161.
[24] H. Bruus, Acoustofluidics 1: governing equations in microfluidics modes, Lab Chip 11 (2011) 3742–3751.

Biographies

H.K. Ma received his PhD degree from the department of mechanical engineering, University of Illinois at Chicago, in 1985. He was a research engineer for Energy and Environmental Research Co. (Irvine, USA) in 1985–1987. He then joined the faculty of the department of mechanical engineering, National Taiwan University, in 1987.

Rong-Huei Chen received his B.S. degree from Nan Jeon University of Science and Technology, Taiwan, in 2008; and received his M.S. degree from Yuan Ze University, Taiwan, in 2010. He is currently a Ph.D. candidate in the Department of Mechanical Engineering, National Taiwan University, Taiwan. He is focused on the piezoelectric materials for novel actuators, particularly piezoelectric micropumps.

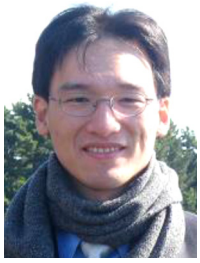

Dr. Yu-Hsiang Hsu is currently an Assistant professor in the Institute of Applied Mechanics and the director of Biomechanical Microsystems Laboratory at National Taiwan University. He received his B.S. degree in Mechanical Engineering and M.S. degree in Applied Mechanics from National Taiwan University in 2000 and 2002, respectively. He then received his M.S. degree and Ph.D. degree in Biomedical Engineering in 2006 and 2010 from the University of California at Irvine. His research interests include biomedical devices, lab-on-a-chip systems, 3D microtissues, and drug screening systems.